Nanosecond Guard Time Packet-by-Packet Burst-Mode Optical 3R Regeneration in an Optical-Label Switching Router

Masaki Funabashi, Zhong Pan, Zuqing Zhu, and S. J. B. Yoo, *Senior Member, IEEE*

***Abstract*—This letter discusses an experimental demonstration of 10-Gb/s packet-by-packet burst-mode optical 3R regeneration in an optical-label switching router. A monolithically integrated Mach–Zehnder interferometer with semiconductor optical amplifiers provides the all-optical 2R regeneration. Synchronous modulation with the use of Fabry–Pérot filter-based clock recovery performs the burst-mode retiming function necessary for 3R regeneration. The clock recovery works successfully despite a clock phase discontinuity between adjacent packets. The optical 3R regenerator shows bit-error rates below 1×10^{-10} and sensitivity variations less than 1.5 dB over a wide range of guard times from 3 to 1000 ns.**

***Index Terms*—Burst-mode clock recovery, Fabry–Pérot filter (FPF), optical packet switching, optical regeneration.**

I. Introduction

OPTICAL packet switching is of great interest due to its potential for flexibility, scalability, and bandwidth efficiency. Optical-label switching (OLS) is an attractive technology that takes advantage of flexible label processing in the electrical domain for routing and forwarding decisions, while achieving high-capacity payload data forwarding in the optical domain [1]. All-optical signal regeneration plays an important role in scalable all-optical networks using OLS routers. Unlike a regenerator in a continuous data stream, one in an asynchronous packet data stream must support burst-mode and packet-by-packet operation because packets with variable lengths will arrive at unpredictable times. Moreover, the capability of handling packets with a short guard time is desired for high throughput.

While 2R regeneration (reamplification, reshaping) is often sufficient when amplitude noise is the major source of signal deterioration [2], the full 3R regeneration functionality (2R + retiming) is necessary for high bit-rate or long-distance transmission systems in which timing jitter accumulations are detrimental [3]. Clock recovery is essential for retiming, and all-optical methods using a Fabry–Pérot filter (FPF) [4]–[8], a self-pulsating multisection distributed feedback (DFB) laser [9], [10], or a mode-locked laser [11], [12] have been reported. Among these methods, the FPF-based technique is most promising because of its rapid response and passive construction [6], [7]. However, the majority of the previous work focused on continuous-mode clock recovery, and several publications reporting burst-mode clock recovery [5], [7], [10] did not incorporate it into a 3R regenerator. Only a few papers discuss 3R regeneration using burst-mode clock recovery [6].

This letter investigates the guard time dependence of burst-mode 3R regeneration utilizing FPF-based clock recovery, which is useful for OLS networks. In order to investigate its performance in OLS networks, we set practical conditions such as guard times ranging from 3 to 1000 ns, a pseudorandom bit sequence (PRBS) of $2^{23} - 1$, the clock phase discontinuity between packets, and various packet lengths.

II. Experimental Setup

The experimental setup utilizes a practical situation in which the burst-mode 3R regenerator is part of an OLS router [2], [13]. Fig. 1(a) shows the experimental setup. A subcarrier-multiplexing transmitter (SCM-Tx1) generates optical packets with 10-Gb/s return-to-zero (RZ) payloads on the baseband and 155-Mb/s nonreturn-to-zero labels on the 14-GHz subcarrier. The label extractor separates the optical label from the payload, and the burst-mode label receiver receives the optical label. The switch-controller makes a decision according to the label content and the forwarding table, and instructs the tunable wavelength converter (TWC) to tune to a new wavelength, which corresponds to the directing of the payload to a desired output port of the arrayed waveguide grating router (AWGR). $(m, n)_{\text{in}}$ and $(m, n)_{\text{out}}$ represent the nth wavelength channel on the mth input and output fiber, respectively. The fixed wavelength converter at the AWGR output converts the payload wavelength to the desired fixed wavelength and applies the burst-mode 3R regeneration function thereto.

The burst-mode 3R regenerator consists of an all-optical 2R regeneration stage and a burst-mode retiming stage [14]. The 2R stage is a wavelength converter based on a Mach–Zehnder interferometer monolithically integrated with semiconductor optical amplifiers (SOA-MZI: Alcatel 1902 ICM), in which the cross-phase modulation effect takes place. The payload signal is split and fed into each arm of the SOA-MZI with a relative delay controlled by the tunable delay line (TDL2), which enables the SOA-MZI to operate in the differential mode, producing a faster device response time than the gain recovery time of the SOAs. The retiming stage includes a burst-mode clock recovery module utilizing a fiber-optic FPF followed by an SOA

Manuscript received December 27, 2005; revised February 24, 2006. This work was supported in part by Furukawa Electric, and in part by the National Science Foundation under NSF 0335301 and NSF 9986665.

M. Funabashi is with the Department of Electrical and Computer Engineering, University of California, Davis, CA 95616 USA, and also with The Furukawa Electric Co., Ltd., Yokohama 220-0073, Japan (e-mail: funa@ece.ucdavis.edu).

Z. Pan, Z. Zhu, and S. J. B. Yoo are with the Department of Electrical and Computer Engineering, University of California, Davis, CA 95616 USA (e-mail: yoo@ece.ucdavis.edu).

Digital Object Identifier 10.1109/LPT.2006.873354

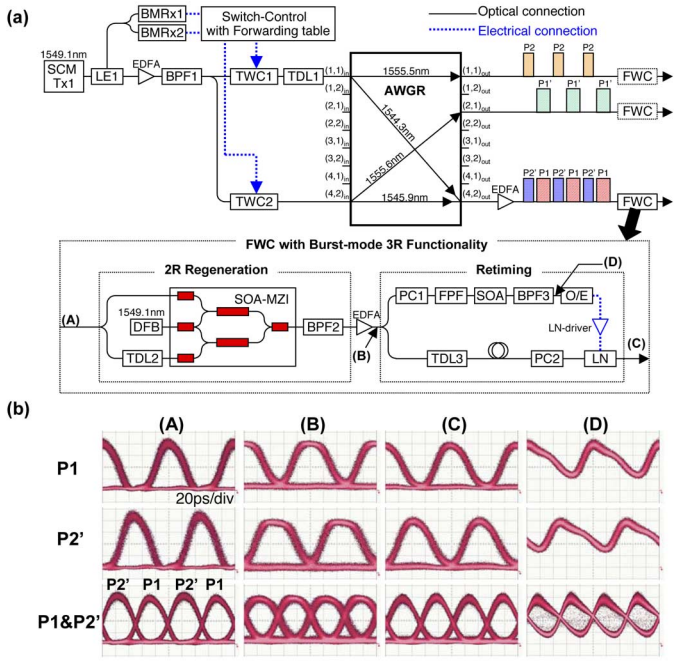

Fig. 1. (a) Experimental setup of the OLS router with the burst-mode 3R regenerator. (b) Eye diagrams of packet P1 and P2' at different locations of (A) before 2R regeneration, (B) after 2R regeneration, (C) after retiming, and (D) after optical clock recovery. (Color version available online at http://ieeexplore.ieee.org.)

[8] and a synchronous modulation module using a $LiNbO_3$ (LN) modulator. The free spectral range of the FPF matches the bit rate of the incoming RZ signal (i.e., 10 GHz), and its finesse is approximately 100. To mitigate the polarization dependence of the FPF, the polarization controller (PC1) aligns the input polarization to one of the two principal axes of the FPF. A thermoelectric cooler with 0.01 °C accuracy aligns the passbands of the FPF to the frequencies of the optical carrier and clock components, generating a clock-like optical signal at the output of the FPF. This clock-like signal exhibits amplitude variations following the pattern of the incoming bit stream. The gain-saturated SOA following the FPF suppresses the amplitude variations. The subsequent bandpass filter (BPF3) transmits the recovered clock signal and suppresses the amplified spontaneous emission noise from the SOA, especially during the guard times. The optical-to-electrical receiver converts the optical clock signal into an electrical signal that modulates the LN modulator after being amplified by the LN driver.

To recover the clock with a short and pattern-independent rise time, we used a preamble of consecutive 16-bit ones ("1"s) followed by PRBS $2^{23}-1$ data to the end of each packet. A preliminary characterization shows that the recovered clock signal has a rise time and a fall time of approximately 1–2 and 4–5 ns, respectively. To make the best use of the clean part of the recovered clock, the fiber length before the LN modulator is adjusted so that the recovered clock signal arrives at the LN earlier than does the payload signal by 2 ns. This adjustment enables the payload signal to interact with the recovered clock signal with a uniform amplitude. The TDL3 aligns the phase between the payload signal and the recovered clock signal.

We experimentally emulated the situation in which two packets with mutually out-of-phase clock cycles arrive at the burst-mode 3R regenerator. The SCM-Tx1 alternatively generates two different packets, P1 and P2, with lengths of 2.1 and 1.6 μs, respectively. The guard times between P1 and P2 (and between P2 and P1) were the same for each experiment, but various guard times, ranging from 3 to 1000 ns, have been tested. For simplicity, we split the output of SCM-Tx1 to emulate two different input packet streams. The TWC1 switched P1 to output port $(4,2)_{\text{out}}$ and P2 to $(1,1)_{\text{out}}$ while TWC2 switched P1' to $(2,1)_{\text{out}}$ and P2' to $(4,2)_{\text{out}}$, generating an alternative packet sequence of P1 and P2' with different packet lengths and wavelengths at the AWGR output port $(4,2)_{\text{out}}$. Through adjustment of the TDL1, the relative clock phase difference between P1 and P2' was set at π (50-ps shift). We consider this case to be the most difficult for burst-mode clock recovery because the recovered clock signal with the opposite phase will suppress mark bits in the synchronous modulation of the retiming stage, especially when the guard time is so short that the trailing part of the recovered clock overlaps with the leading part of the following packet.

III. Experimental Results

Fig. 1(b) shows eye diagrams measured at points (A), (B), (C), and (D) of Fig. 1(a) when the pure PRBS $2^{23}-1$ pattern is used as a payload signal. Eye diagrams in the first and the second row are measured for P1 and P2', respectively. Eye diagrams in the third row are measured by overlapping the P1 eyes and P2' eyes on the display aligned in time with the use of the local clock trigger. The difference in the pulse peak positions of P1 and P2' is the result of the relative clock phase difference of π (50 ps), and the results indicate that the clock recovery can follow the phase discontinuities and operate in a packet-by-packet burst mode. The pulse shape after 2R regeneration is intentionally broadened in time to realize a relatively flat mark level to facilitate synchronous modulation in the retiming stage. Here, the recovered clock carves off the edges of the broadened pulse for retiming. The eye diagrams after the retiming exhibit clear eye openings and high extinction ratios. The dots in the optical clock eye diagram shown in the third row of Fig. 1(b), column (D), are mainly due to the amplified transient clock signal during the guard times ($P1 \rightarrow P2'$ or $P2' \rightarrow P1$). These dots are not present in the clock eye diagrams of P1 or P2' when they are measured separately.

We measured bit-error-rate (BER) curves at three locations: before and after the 2R stage and after the retiming stage. Fig. 2(a) shows the BER curves for packet P1 when the guard times are 3 and 20 ns. The BER measurement uses the local clock trigger from the BER tester, and errors are counted for all of the bits in P1, including the 16-bit preamble. The BER curves show error-free performances below 1×10^{-10}. Similar error-free operation is confirmed for P2'. In order to examine the 3R performance at various guard times, Fig. 2(b) plots the received optical power (receiver sensitivity) at BER $=1\times10^{-9}$ versus the guard time. The variations in receiver sensitivity are less than 1.5 dB throughout the guard time range of 3–1000 ns.

Fig. 3(a) shows a bit pattern with a 3-ns guard time, in which the measured guard time is 3.0 ns followed by the preamble. Fig. 3(b) and (c) shows the trailing and leading parts of packets before and after the 3-ns guard time, respectively. Fig. 3(d) is the leading part of packet P1 when the guard time is 20 ns. Although there are no significant differences in the BER results in Fig. 2(a), the pulsewidths of the earlier bits are broader than

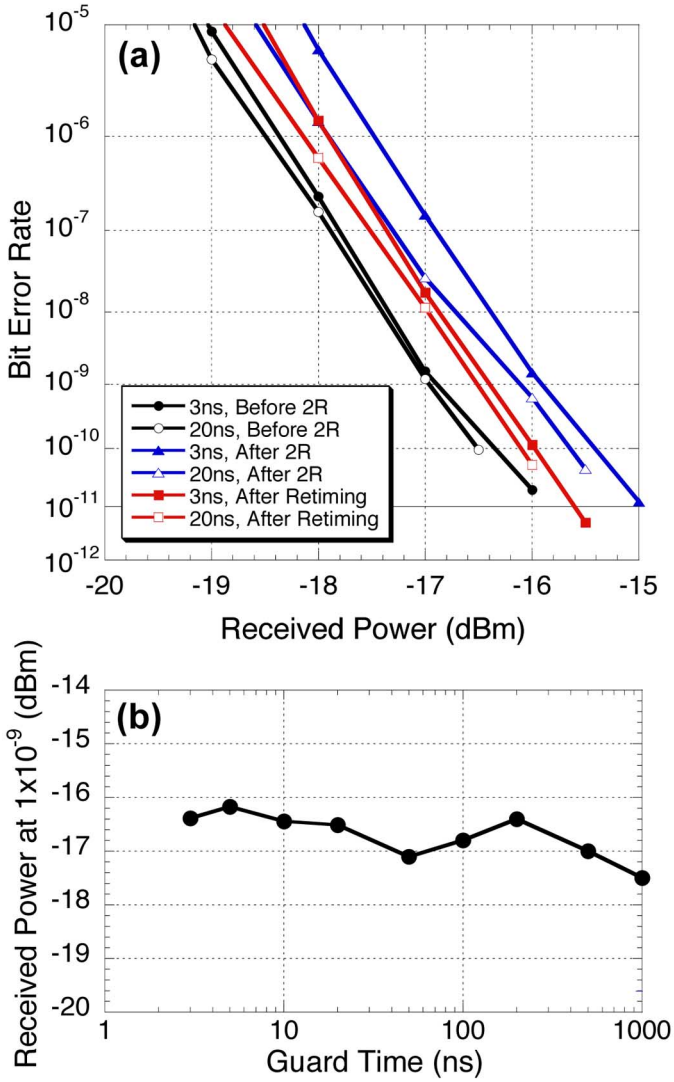

Fig. 2. (a) BER curves at each stage for 3- and 20-ns guard times. (b) Received power levels at BER $= 1 \times 10^{-9}$ for guard times from 3 to 1000 ns. (Color version available online at http://ieeexplore.ieee.org.)

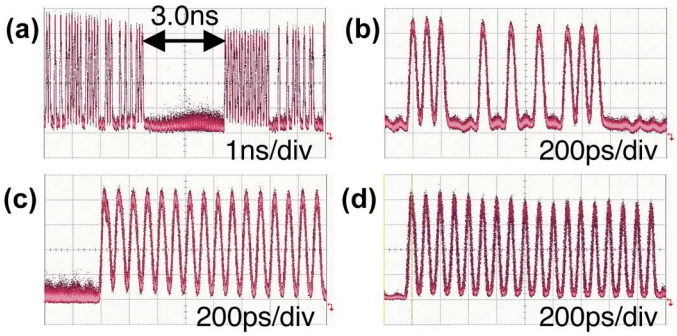

Fig. 3. Bit patterns measured after the retiming stage. (a) Bit pattern around 3-ns guard time between P2' and P1. (b) Trailing part of packet P2'. (c) Leading part of packet P1. (d) Leading part of packet P1 for 20-ns guard time. (Color version available online at http://ieeexplore.ieee.org.)

those of the later bits in Fig. 3(c), whereas the pulsewidths are almost constant in Fig. 3(d). These results occur because the trailing part of the recovered clock from the previous packet with an opposite phase (π) destructively interferes with the recovered clock from the current packet, which results in a reduced clock amplitude and a smaller modulation depth in the synchronous modulation of the retiming stage.

We also experimentally verified that the tuning of TDL1 over one bit period (100 ps) showed no observable difference in the measured BER values, which indicates that the 3R regenerator works properly regardless of the degree of the phase difference between the two packets. The phase noise measurement of the recovered optical clock showed a maximum root-mean-square jitter of 0.342 ps for continuous PRBS $2^{23} - 1$ data.

IV. Conclusion

We have demonstrated nanosecond guard time 10-Gb/s burst-mode 3R regeneration, combining SOA-MZI-based all-optical wavelength conversion and synchronous modulation using FPF-based clock recovery. The experiments utilized the OLS router to emulate practical situations with various guard time values, π clock phase discontinuity between adjacent packets, diverse packet lengths and wavelengths, and PRBS $2^{23}-1$ data streams. The burst-mode optical 3R regenerator showed BER below 1×10^{-10} without an error-floor, as well as small sensitivity variations of less than 1.5 dB throughout a guard time range from 1000 ns down to 3 ns. The results indicate that the demonstrated 3R regenerator has burst-mode capability under practical situations.

References

[1] B. Meagher *et al.*, "Design and implementation of ultra-low latency optical label switching for packet-switched WDM networks," *J. Lightw. Technol.*, vol. 18, no. 12, pp. 1978–87, Dec. 2000.

[2] M. Y. Jeon *et al.*, "Demonstration of all-optical packet switching routers with optical label swapping and 2R regeneration for scalable optical label switching network applications," *J. Lightw. Technol.*, vol. 21, no. 11, pp. 2723–2733, Nov. 2003.

[3] G. Raybon *et al.*, "40 Gbit/s pseudo-linear transmission over one million kilometers," in *Proc. OFC 2002*, Anaheim, CA, Postdeadline Paper FD10.

[4] M. Jinno *et al.*, "All-optical timing extraction using an optical tank circuit," *IEEE Photon. Technol. Lett.*, vol. 2, no. 3, pp. 203–204, Mar. 1990.

[5] C. Bintjas *et al.*, "Clock recovery circuit for optical packets," *IEEE Photon. Technol. Lett.*, vol. 14, no. 9, pp. 1363–1365, Sep. 2002.

[6] G. T. Kanellos *et al.*, "Clock and data recovery circuit for 10-Gb/s asynchronous optical packets," *IEEE Photon. Technol. Lett.*, vol. 15, no. 11, pp. 1666–1668, Nov. 2003.

[7] L. Stampoulidis *et al.*, "40 Gb/s fast-locking all-optical packet clock recovery," in *Proc. OFC/NFOEC 2005*, vol. 4, Anaheim, CA, Paper OThE2.

[8] G. Contestabile *et al.*, "40-GHz all-optical clock extraction using a semiconductor-assisted Fabry–Pérot filter," *IEEE Photon. Technol. Lett.*, vol. 16, no. 11, pp. 2523–2525, Nov. 2004.

[9] C. Bornholdt *et al.*, "Self-pulsating DFB laser for all-optical clock recovery at 40 Gbit/s," *Electron. Lett.*, vol. 36, pp. 327–328, 2000.

[10] I. Kim *et al.*, "Dynamics of all-optical clock recovery using two-section index- and gain-coupled DFB lasers," *J. Lightw. Technol.*, vol. 23, no. 4, pp. 1704–1712, Apr. 2005.

[11] K. Smith and J. K. Lucek, "All-optical clock recovery using a mode-locked laser," *Electron. Lett.*, vol. 28, pp. 1814–1816, 1992.

[12] H. Yokoyama *et al.*, "Highly reliable mode-locked semiconductor lasers and their applications," in *Proc. CLEO/Pacific Rim*, vol. 2, 2001, pp. 498–499.

[13] S. J. B. Yoo *et al.*, "Rapidly switching all-optical packet routing system with optical-label swapping incorporating tunable wavelength conversion and a uniform-loss cyclic frequency AWGR," *IEEE Photon. Technol. Lett.*, vol. 14, no. 8, pp. 1211–1213, Aug. 2002.

[14] M. Funabashi *et al.*, "All-optical 3R regeneration in monolithic SOA-MZI to achieve 0.4 million km fiber transmission," in *Proc. LEOS Ann. Meeting*, 2005, pp. 137–138.